IMPULSE FORCE INVESTIGATIONS OF STRAIN GAUGE SENSORS

Michael Kobusch[1], Thomas Bruns[1], Lioba Stenner[2], Sven-Patrick Schotte[2]

[1]Physikalisch-Technische Bundesanstalt (PTB), Braunschweig, Germany
[2]Hottinger Baldwin Messtechnik GmbH (HBM), Darmstadt, Germany

ABSTRACT

This paper presents new investigations of strain gauge force sensors subject to impulse loads. Different approaches regarding the determination of the fundamental axial resonance are discussed in order to get information about a practical evaluation method for common-type strain gauge sensors under dynamic loads.

1. INTRODUCTION

The demand for precise impulse force measurements is steadily increasing due to the rising number of dynamic applications. Here, although not primarily designed for dynamic loads, strain gauge based force transducers are widely used and play an important role on the market. Investigations of force transducers with sine forces prove a frequency-dependent behaviour which is primarily determined by the inner construction and the type of force introduction. Due to the fact that an impulse excitation has a continuous frequency spectrum and not just a single line, the analysis of impulse force measurements is even more complex. Even though force transducers are used to measure dynamic forces, it is still standard industrial practice to calibrate such transducers under static conditions only. Therefore, the true measurement uncertainties are not well known.

The useable frequency range of a strain gauge sensor is limited by its structural resonance behaviour which results from the geometrical mass distribution and the material's mechanical properties. A first step towards the dynamical characterisation of a sensor is the specification of the fundamental resonant frequency, as proposed in the German guideline VDI/VDE 2638. This resonance is defined as the axial vibration of the unloaded sensor fixed at its base and not coupled to any other mechanical parts. Using the simplification of the spring-mass-model depicted in Fig. 1, the sensor's top mass m_{top} and the axial compliance c describe the fundamental resonant frequency according to

$$f_{\mathrm{res}} = 1/(2\pi) \cdot \sqrt{1/(c \cdot m_{\mathrm{top}})} \cdot$$

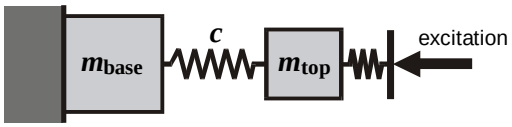

Figure 1: Spring-mass-model of a force sensor

It is easily understood that a coupling of additional masses changes the dynamic behaviour. In this case, the sensor's compliance and top mass should be specified individually in order to allow an estimation of the changed axial resonance.

In the following, computational results from a finite element (FE) simulation are compared to different experimental methods for the determination of the fundamental resonance. One

method makes use of static measurements for the displacement at nominal load and for the weight force of the top mass. Another method analyses the impulse response of hammer excitation. Furthermore, measurements at the 20 kN Impact Force Standard Machine (IFSM) complete this comparison.

2. FORCE SENSORS

Three different types of 10 kN strain gauge force sensors manufactured by HBM were tested for this study (Fig. 2). The sensors are made of stainless steel and have base diameters of 50 mm. They are typically used for various industrial applications. The HBM C2 is for compressive forces only, the types U2B and U3 measure tensile forces as well. Tensile forces are introduced over a central threaded connector (U2B) or a flange (U3), respectively, whereas the base of the sensor is fixed by screws. Beside their different load connectors, the types C2 and U2B have a similar structural design. The special design of the type U3 features an integrated lateral force compensation which allows high lateral load components. In each case, the sensor housing is part of the axisymmetric elastic spring element applied with strain gauges at its bottom surface (cf. Fig. 3).

HBM C2 / 10 kN HBM U2B / 10 kN HBM U3 / 10 kN

Figure 2: Investigated HBM force sensors of 10 kN nominal load

For comparable loading conditions in the experimental tests, forces were introduced over a spherical load button in all cases. Whereas the threaded connector of the U2B already bears a spherical top of 60 mm radius, a load adapter had to be manufactured for the U3.

3. FINITE ELEMENT MODELLING

For each sensor, a finite element (FE) model was generated from its geometrical CAD-data. In order to obtain simplified 3D-models of rotational symmetry, details and asymmetries like bore-holes were omitted. Figure 3 visualises the cross-sectional views of the modelled sensors. The type U3 was modelled with and without its load adapter, whereas the removable base adapter of the U2B shown in Fig. 2 was not included. For the volume meshing, second order elements using 20 nodes were applied.

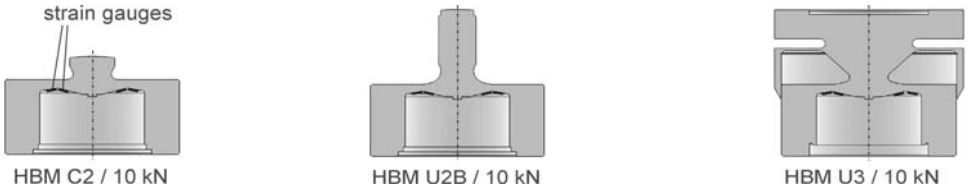

Figure 3: Cross-sectional view of the modelled force sensors

The elastic deformation at nominal load was calculated by a static structural analysis. To avoid the complex modelling of the contact problem, the load was applied as a uniform pressure acting on the curved surface of the load button. Thus, the FE calculation could only supply information about the structural deformation. If necessary, the additive contribution of the

elastic contact was considered, too. It can be calculated with the well-known Hertzian formulas. The results of the structural FE analyses are summarised in Table 1. Two (or three) values for the deformation at 10 kN nominal load are given, namely the axial displacement of the surface under load and the axial flexure of the force measuring membrane. It becomes apparent that all sensors use a membrane of similar flexure. The axial displacement at the top, i.e. load button (C2, U2B) or flange ring (U3), is higher and depends on the sensor type. This means that a substantial part of the sensor's total compliance is caused by the elasticity of the top mass itself and not only by the force measuring membrane.

Table 1: FE-calculated elastic deformations at 10 kN nominal load:
axial displacement of the top surface, of the flange ring (for U3), axial flexure of the measuring spring membrane.

C2 / 10 kN		**U2B / 10 kN**		**U3 / 10 kN**		
top	membrane	top	membrane	top of load adapter	flange ring	membrane
0.0416 mm	0.374 mm	0.0532 mm	0.0378 mm	0.0602 mm	0.0460 mm	0.0371 mm

The top masses of the investigated transducers were estimated from their geometrical data. Here, the separation between top mass and base mass was placed at the thinnest part of the membranes. The results of this idealisation are given in Table 2. In addition, the table lists the estimations for the fundamental resonance evaluated from the simplified spring-mass-model. The small top masses of the C2 and U2B lead to high frequencies, whereas the higher mass of the U3 results in a much lower frequency.

Table 2: Top masses estimated from geometrical data and evaluated fundamental resonant frequencies

C2 / 10 kN		**U2B / 10 kN**		**U3 / 10 kN**		incl. load adapter	
14.9 g	21.3 kHz	25.0 g	16.4 kHz	200.3 g	5.84 kHz	337.5 g	4.50 kHz

A more precise method for the computational investigation of structural resonances is the modal FE analysis. For the modelled force sensors, Table 3 lists their first modal frequencies and gives a short description of the respective modal forms. All calculations were performed for two mounting conditions, for a fixed and for a free base, respectively. In any case, the lowest resonance characterises a bending mode. The interesting fundamental axial resonance of the sensor's top mass is marked in boldface. The values agree quite well with those of Table 2 derived from the simplified spring-mass-model. The maximum relative deviation amounts to 9 % for the U3 type, the best agreement is obtained for the C2 with less than 0.5 %. In addition, the two mounting conditions have different mode patterns. The axial resonance of a free sensor is always higher than that of a sensor with fixed base. The relative deviation is very pronounced for the U3 with its heavy top mass.

Table 3: FE-calculated first modal frequencies:
axial resonance of top mass (ax), bending of housing (be), bending of load button (bl), buckling of membrane (bu), torsion (to), vibration of housing (ho)

C2 / 10 kN		**U2B / 10 kN**		**U3 / 10 kN**		incl. load adapter
base fixed	base free	base fixed	base free	base fixed	base free	base fixed
20.4 kHz (be)	15.1 kHz (ho)	7.93 kHz (bl)	8.71 kHz (bl)	2.76 kHz (be)	4.67 kHz (be)	1.80 kHz (be)
21.4 kHz (ax)	**22.4 kHz (ax)**	**15.9 kHz (ax)**	15.1 kHz (ho)	**5.32 kHz (ax)**	**7.10 kHz (ax)**	**4.17 kHz (ax)**
31.4 kHz (bu)	28.1 kHz (ho)	20.6 kHz (be)	**17.0 kHz (ax)**	6.33 kHz (to)	8.14 kHz (to)	4.88 kHz (to)
31.9 kHz (to)	31.3 kHz (bu)	29.3 kHz (to)	27.8 kHz (ho)	9.68 kHz (be)	14.6 kHz (be)	8.59 kHz (be)

4. MEASUREMENTS OF COMPLIANCE AND TOP MASS

The sensor's fundamental resonance can be estimated by static measurements readily available at the manufacturer's lab. Examples of such measurements performed at HBM are shown in Fig. 4 for an U3 type sensor under test. At left, the displacement at nominal load is measured by a

dial gauge touching the spot of interest. The gauge was rigidly fixed at the base plate supporting the sensor. The photograph at right shows a measurement of the weight force of the sensor's top mass.

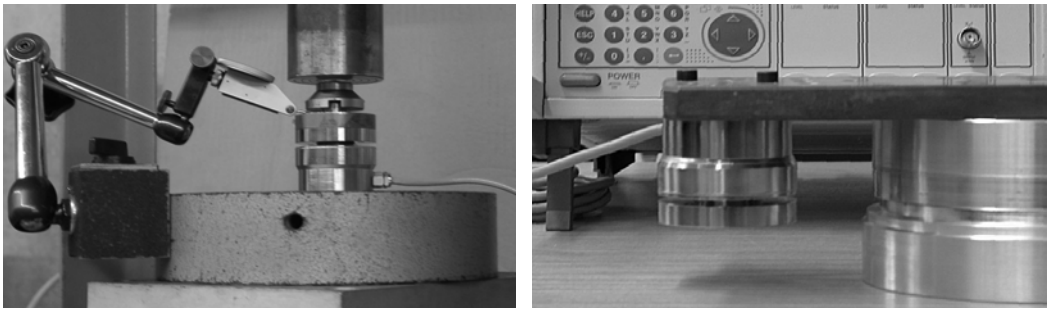

Figure 4: Measurement of the sensor's compliance (left), measurement of the weight force of the top mass (right)

According to the German guideline VDI/VDE 2638, the nominal displacement is defined as the displacement of the contacting coupling elements at nominal load. This implies that the elasticity of the mechanical contact itself may contribute substantially. In this case, the force measuring spring is not very well described by the total displacement. Nevertheless, the compliance of the contact between a spherical surface of radius R (load button) and a plane surface can be estimated by using the Hertzian formulas. Figure 5 visualises the non-linear relation between force F and elastic displacement x (approach of the contact surfaces), plotted for the values of the investigated sensors (R=60 mm, steel-steel material combination). The given formula assumes bodies of the same material (modulus of elasticity E, Poisson ratio).

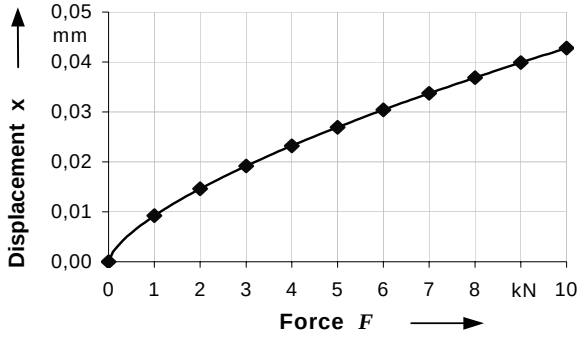

$$F = \frac{2\,E}{3\,(1-\mu^2)} \cdot \sqrt{R\,x^3}$$

Figure 5: Hertzian contact of a spherical (R = 60 mm) and plane surface of bodies made of steel

At 10 kN nominal load, following load-induced displacements were measured: total displacement of 0.08 mm (C2) and 0.11 mm (U2B) including Hertzian contact, displacement at the flange ring of 0.05 mm (U3). The uncertainties with the applied equipment was about 0.01 mm. Nevertheless, the measured values agree well with the FE-calculated values of Table 1, if the Hertzian contact displacement of about 0.043 mm is taken into account (for C2, U2B).

In the second investigation, the top mass of a sensor was measured by simply turning the sensor with its vertically orientated axis upside down. In this case, the indicated difference signal expresses the doubled weight force of the top mass. Results achieved with five repetitive measurements are listed in Table 4. The tests were performed with an ML38 amplifier connected to an MGCplus system. The listed values differ somewhat from those derived from geometrical data (cf. Table 2). As expected, the observed repeatability was not good, because the measurements were taken at only 0.002 % (0.02 % for U3) of the nominal load of 10 kN. This was confirmed by a DKD calibration according to ISO 376 with only 20 N maximum load and 8 load steps performed with the U2B / 10 kN. At the smallest load step of 2.5 N, the

observed uncertainty (k=2) corresponds to a mass of 14 g. This result reveals that the described method for the experimental determination of the top mass bears high uncertainties.

Table 4: Top masses derived from its measured weight force

C2 / 10 kN	U2B / 10 kN	U3 / 10 kN
17.8 g, std. dev. 1.8 g	22.9 g, std. dev. 2.6 g	190 g, std. dev. 5.9 g

Nevertheless, using the experimental results for top mass and estimated membrane compliance, the following fundamental resonant frequencies were calculated: 19.6 kHz (C2), 12.8 kHz (U2B), 5.2 kHz (U3). Considering the high uncertainties involved for the measurement of compliance and top mass, the deviations from the computational modal analysis may not be significant.

5. ANALYSIS OF HAMMER EXCITATIONS

Experiments with hammer excitation were performed in order to measure the fundamental axial resonance of the force sensors. According to the German guideline VDI/VDE 2638, the base of the sensor under test was mounted on a sufficiently big mass, which was the 10 kg mass cube of the IFSM. The strokes were performed with a hand-held hammer. As expected, the excitation of the axial resonance succeeded only with sufficiently hard hammer tips. Hammer tips made of plastics generated considerably long pulses that could not excite the high resonant frequencies of the C2 and U2B type sensors. Typical responses resulting from a hammer excitation using a hammer head of 100 g mass are shown in Fig. 6. The diagrams visualise the spectral contents of the signal ringing evaluated by an FFT analysis. For comparison purposes, the plotted amplitude is normalised to the most intensive spectral line. Furthermore, the inlets show the corresponding time series of the force signal sampled at 100 kS/s. Here, the force peaks of 0.16 ms duration have to be truncated for the C2 and U2B. Due to the overall damping of the signal ringing, only a short time span could be applied to an FFT analysis of low resolution. The observed ringing contains more than one frequency component in most cases. Furthermore, their relative amplitudes change significantly over time which complicates the interpretation of the spectral data.

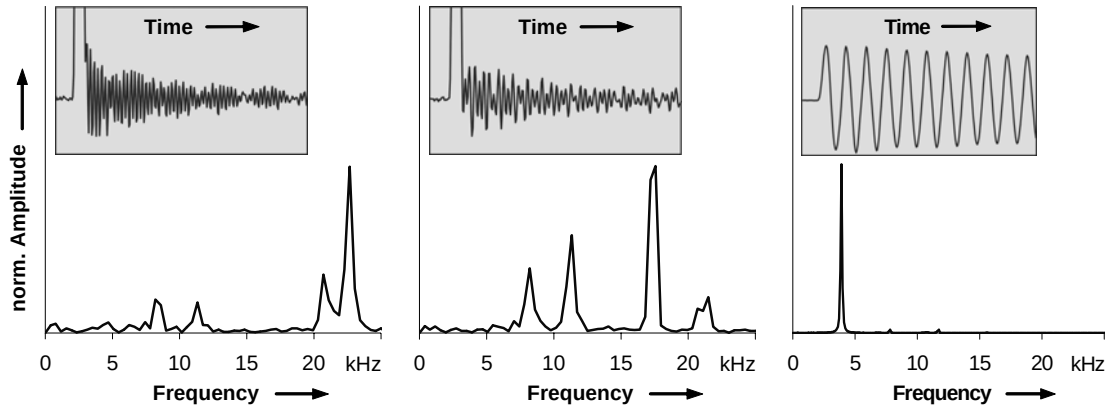

Figure 6: Signal ringing excited by a hammer pulse for three sensors: spectral analysis, time series (inlet) spanning 3 ms

Table 5: Frequency components of the signal ringing excited by a hammer pulse:
FFT frequency resolution of 0.4 kHz (C2, U2B) or 0.2 kHz (U3)

C2 / 10 kN	**U2B / 10 kN**	**U3 / 10 kN**	incl. load adapter
8.2 kHz, 11.3 kHz, 20.7 kHz, 22.7 kHz	8.2 kHz, 11.3 kHz, 17.6 kHz, 21.5 kHz	5.1 kHz	3.9 kHz

For the C2 type, two prominent components are found between 20 kHz and 25 kHz. This agrees with the FE simulation (cf. Table 3) which reveals a bending mode and the fundamental axial resonance in this range. The measurements proved two further components around 10 kHz which have not been predicted by the FE analysis. Their sources are not yet verified. For the U2B type, four components are found in the signal ringing, too. In comparison with the FE results, the component at 17.6 kHz can be identified as the axial resonance. The component at 21.5 kHz may be a bending mode. Two prominent components around 10 kHz are also found in the ringing signal of the U2B. Their relative amplitudes in respect of the 17.4 kHz resonance change from case to case. One of them probably is the bending mode of the threaded load button (c.f. Table 3). The reason for the additional resonances of the C2 and U2B is supposed to be found in the adaptation of the sensor to the 10 kg mass, where a mounting adapter with additional masses and compliances has to be taken into account. Here, further experimental tests and FE investigations are necessary in order to identify the resonant modes. In contrast to the multi-component ringing of the C2 and U2B, only the fundamental axial resonance at 3.9 kHz (5.1 kHz without load adapter) was excited for the U3. These experimental values are in good agreement with the computational values from the finite element model.

6. MEASUREMENTS WITH THE IMPACT FORCE STANDARD MACHINE

The Impact Force Standard Machine (IFSM) of PTB [1] performs traceable calibrations of impulse forces up to 20 kN amplitude (Fig. 7). Impulse forces are generated by a collinear impact of two cube-shaped bodies of 10 kg mass which are guided by linear air bearings. Traceability of force is realised by the determination of mass and acceleration, where the latter is derived from the velocity signal of a laser-Doppler interferometer (vibrometer) [2-3].

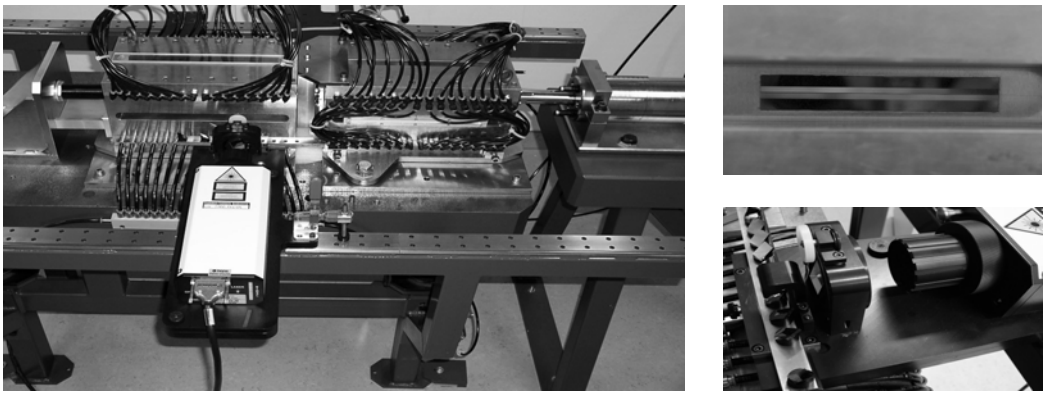

Figure 7: 20 kN Impact Force Standard Machine**:**
(a) impact facility with collinear air bearings, vibrometer in the foreground, acceleration mechanism at right,
(b) double grating (groove spacing 1 m and 0.8 m) applied at the lateral side of a mass cube,
(c) beam deflection mechanism: rail with deflection mirrors (at left), beam displacer (at centre), vibrometer (at right)

Differing from the design previously published [1], some important modifications have been introduced. First, the retro-reflection of the measuring laser beam in Littrow-configuration is now achieved by new diffraction gratings glued onto the lateral sides of the mass cubes (Fig. 7b). The highly reflective Cr-gratings on a thin silicon wafer were manufactured in the clean room facility of PTB. The design features a double grating (groove spacing 1 m and 0.8 m)

in order to be more flexible. Five different beam angles with corresponding scale factors for the measured line-of-sight velocity component allow an optimised utilisation of the vibrometer's measurement ranges. The second modification concerns the mounting rail of the vibrometer. Due to the small number of discrete beam angles, the formerly used bow-shaped mounting rails for unlimited angle adjustment were replaced by linear mounting rails using a beam deflection optics (Fig. 7c). Here, different beam angles are realised by individual beam deflection mirrors. An adjustable beam displacer selects the desired grating. Furthermore, the movable carriage of the vibrometer allows much better access to different measurement locations than before. A third improvement for higher precision is achieved by the analysis of the sampled RF converted interferometer signals. Whereas the uncertainty of the analogue velocity signal is about 1 %, traceability of the new method is based on frequency and laser wavelength and both can be measured very well. A detailed report about the new data acquisition and processing techniques is given in [4]. Nevertheless, traceability is not the primary concern of the study presented here. Different to the hammer excitation, the IFSM generates reproducible force pulses of well-defined axial direction, where parasitic lateral load components are excited to a much lesser extent.

Experimental tests with the three force sensors were performed with maximum pulse forces close to nominal load. For all sensors, the colliding mass cubes generated a pulse force of a duration of 0.6 ms, additional pulse shapers were not used. Figure 8 shows the measured force signals and the corresponding spectral analyses of the signal ringing. The observed frequency components are additionally listed in Table 6.

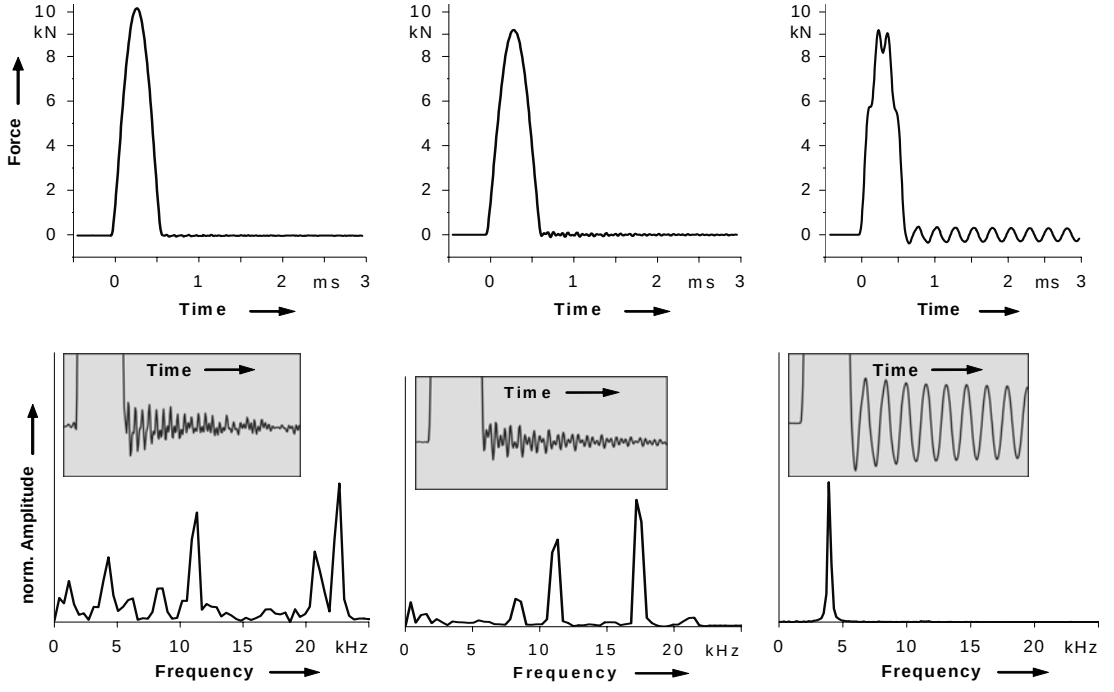

HBM C2 / 10 kN

HBM U2B / 10 kN adapter

HBM U3 / 10 kN with load

Figure 8: Impulse forces measured at the IFSM for three force sensors:
force signals (upper row), spectral analysis of the signal ringing (lower row) with time series spanning 3 ms (inlet)

Table 6: Frequency components of the signal ringing measured at the IFSM:
FFT frequency resolution of 0.4 kHz (C2, U2B) or 0.2 kHz (U3)

C2 / 10 kN	U2B / 10 kN	U3 / 10 kN incl. load adapter
1.2 kHz, 4.3 kHz, 8.6 kHz, 11.3 kHz, 20.7 kHz, 22.7 kHz	8.2 kHz, 11.3 kHz, 17.2 kHz	3.9 kHz

The spectral analyses of the ringing components of the force pulses measured at the IFSM agree quite well with those obtained with a hammer excitation. Remarkably, measurements with the C2 revealed further resonances at low frequencies. The sources of these resonances have to be further analysed. A reason for their absence in the spectra obtained with the 100 gram hammer may be found in the shorter excitation pulse containing less low-frequency components. Furthermore, different constraints of the air-guided mass cube could result in resonances previously not existent. Comparing the relative maximum amplitude of the force peak and the post-impact ringing, this normalised ringing was smaller with the IFSM than before with hammer excitation, namely only 0.4 % for the C2. Measurements with the U3 type sensor with mounted load adapter clearly confirmed the frequency component of the axial resonance at 3.9 kHz. The superposed oscillation of the axial resonance leads to a distorted shape of the acting force pulse.

CONCLUSIONS

The evaluation and assessment of force sensors for dynamic applications has to consider their type-specific resonant behaviour. In order to estimate the sensor's dynamic range, different approaches for the experimental determination of the fundamental axial resonant frequency were discussed. A rough estimation can be made by static measurements of the sensor's compliance and top mass. Dynamic measurement with impulse forces showed that it is quite difficult to extract the right information when parasitic resonances are excited to a greater extend. Consequently, an erroneous identification of the wanted resonant frequency leads to an incorrect specification of the sensor's dynamic range. Here, valuable information can be obtained by a modal FE analysis which also opens new horizons for the manufacturer in order to optimise the mechanical designs with respect to dynamics. Considering the fact that a coupling of additional masses significantly changes the dynamical behaviour, the sole specification of the fundamental resonance is not sufficient. Therefore, it is recommended to specify three additional parameters, namely the compliance of the measuring spring and the masses of the sensor's base and top, which would supply the basic information needed to estimate the dynamics of a sensor coupled to a complex mechanical structure.

REFERENCES

[1] M. Kobusch, Th. Bruns, "The New Impact Force Machine at PTB", *Proceedings of the XVII IMEKO World Congress*, June 22-27, 2003, Dubrovnik, Croatia, pp. 263-267.

[2] Th. Bruns, M. Kobusch, "Impulse Force Calibration: Design and Simulation of a New Calibration Device", *Proceedings of the 17th International Conference on Force, Mass, Torque and Pressure Measurements, IMEKO TC3*, 17-21 Sept. 2001, Istanbul, Turkey, pp. 85-91.

[3] Th. Bruns, R. Kumme, M. Kobusch, M. Peters, "From oscillation to impact: the design of a new force calibration device at PTB", *Measurement*, **32**, pp. 85-92, 2002.

[4] Th. Bruns, M. Kobusch, "Data Acquisition and Processing for PTB's Impact Force Standard Machine", *IMEKO TC 3*, Cairo, Egypt, 2005, to be published.

Addresses of the Authors:

Dr. Michael Kobusch, FB 1.3 (Department of Kinematics) , Physikalische-Technische Bundesanstalt (PTB), Bundesallee 100, 38116 Braunschweig, Germany, michael.kobusch@ptb.de

Dr. Thomas Bruns, FB 1.3 (Department of Kinematics) , Physikalische-Technische Bundesanstalt (PTB), Bundesallee 100, 38116 Braunschweig, Germany, thomas.bruns@ptb.de

Lioba Stenner, Hottinger Baldwin Messtechnik GmbH (HBM), Im tiefen See 45, 64293 Darmstadt, Germany, lioba.stenner@hbm.com

Sven-Patrick Schotte, Hottinger Baldwin Messtechnik GmbH (HBM), Im tiefen See 45, 64293 Darmstadt, Germany, sven.schotte@hbm.com